npj | Quantum Materials

www.nature.com/npjquantmats

REVIEW ARTICLE OPEN

Topological insulators for thermoelectrics

Ning Xu[1], Yong Xu[2,3,4] and Jia Zhu[1]

Topological insulators demonstrate tremendous potential in fields of electronics and magnetism for their unique boundary states that are topologically protected against backscattering at non-magnetic impurities and defects. Intriguingly, most topological insulators are also excellent thermoelectric materials, since topological insulator and thermoelectric compounds share similar material features, such as heavy elements and narrow band gaps. While the influence of topological insulator boundary states has long been neglected in early thermoelectric research, recently this neglected issue has attracted intensive research efforts. A lot of theoretical and experimental investigations have emerged to explore the contribution of topological insulator boundary states to thermoelectricity. Here, we will review the most updated theoretical and experimental progresses, trying to offer a comprehensive understanding on the relation between thermoelectric properties and topological nature. Special emphasis will be laid on the potential of topological states for improving thermoelectric properties, to pave a new way of realizing high-performance thermoelectric devices.

npj Quantum Materials (2017)2:51 ; doi:10.1038/s41535-017-0054-3

INTRODUCTION

Thermoelectric (TE) materials which are capable of direct energy conversions between heat and electricity are of great significance in energy field, for their advantages over conventional ways in refrigeration and power generation as follows: solid-state devices with no moving parts, no environmentally harmful fluids, no noise disturbance, no placement angle limit and no gravity limit; no need for maintaining large temperature difference so that can be used to recover waste heat in various occasions; long and reliable working life at low cost; precise temperature control.[1, 2] Besides these traits, they can be scalable, lightweight, and even made into micro/nano devices to realize local cooling/heating or power generation.[3]

The efficiency of TE materials is determined by the dimensionless figure of merit $ZT = (S^2\sigma/\kappa)T$, where S, σ, κ, and T are, respectively, the Seebeck coefficient, electrical conductivity, thermal conductivity, and absolute temperature.[1, 2, 4] To achieve excellent TE performances, a high ZT value is desirable, which expects a large thermopower (the absolute value of S), a high electrical conductivity and a low thermal conductivity at the same time. However, the optimization of ZT represents a grand challenge in material sciences, because these three comprising parameters are conflictingly correlated and cannot be tuned independently.[5] As a result of continuing efforts for decades, various innovative approaches and concepts have been developed to enhance TE performance, such as alloying, nano-engineering, band convergence, energy filtering, and hierarchical architecturing.[6–16]

Topological insulators (TIs) have attracted a lot of attention on the horizon of condensed matter physics and materials science for their possession of gapped bulk states and gapless Dirac boundary states simultaneously.[17, 18] These non-trivial boundary states, including edge states of two-dimensional (2D) TIs and surface states of three-dimensional (3D) TIs, originated from intrinsic bulk properties such as spin–orbit coupling, band inversion, and bulk bands of opposite parities, are topologically protected by time reversal symmetry of the materials. The edge states are one-dimensional (1D) metallic, wrapping around the 2D materials, and in such states, counter-propagating electrons show opposite spin directions, as depicted in Fig. 1a. The surfaces states are 2D metallic, surrounding the entire materials, in which electrons also show momentum-dependent spin direction, as shown in Fig. 1b. Due to the topological protection, the spins of Dirac fermions are tightly locked with their momentum, thus the charge carriers on the boundary states of TIs experience no backscattering at impurities and defects, beneficial for low-dispassion transport.

Very importantly, a lot of TIs are excellent TE materials, such as bismuth telluride (Bi_2Te_3), antimony telluride (Sb_2Te_3), bismuth selenide (Bi_2Se_3), tin telluride (SnTe) and so on,[19–23] since TE and TI compounds typically favor similar material features, such as heavy elements and narrow band gaps. Therefore, it is a natural question to ask whether the TI boundary states could bring in improved TE performance. Various theoretical and experimental studies have emerged, trying to figure out the contribution of TI boundary states to thermoelectricity.

There already exist some published review papers about TE and TIs, which focus on describing compound classes,[24] or discussing typical TE properties of TIs with gapless boundary states.[25] It is well known that in TI nanostructures, the boundary states from opposite sides are able to overlap in real space and get hybridized with each other. This could introduce a hybridization gap in the otherwise gapless boundary states, thus significantly affecting TE properties. Herein we will offer a colloquium on the most updated studies of TE performance of TI nanostructures without and with the hybridization effect, including recent progresses from both theoretical and experimental sides. When the hybridization effect

[1]National Laboratory of Solid State Microstructures, College of Engineering and Applied Sciences, and Collaborative Innovation Center of Advanced Microstructures, Nanjing University, Nanjing 210093, China; [2]State Key Laboratory of Low Dimensional Quantum Physics, Department of Physics, Tsinghua University, Beijing 100084, China; [3]Collaborative Innovation Center of Quantum Matter, Beijing 100084, China and [4]RIKEN Center for Emergent Matter Science (CEMS), Wako, Saitama 351-0198, Japan
Correspondence: Yong Xu (yongxu@mail.tsinghua.edu.cn) or Jia Zhu (jiazhu@nju.edu.cn)

Received: 11 February 2017 Revised: 15 June 2017 Accepted: 25 July 2017
Published online: 07 September 2017

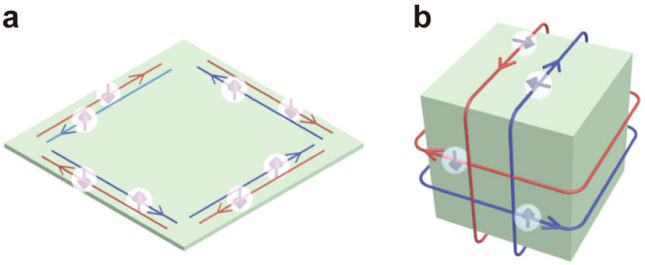

Fig. 1 **a** Schematic of 1D metallic edge states wrapping along the edges of 2D TIs. **b** Schematic of 2D metallic surface states covering the entire surfaces of 3D TIs. *Red* and *blue* colored lines represent counter-propagating electrons with opposite spins (denoted by *arrows*)

is minimized, topologically protected boundary states can serve as superior conducting channels.[26, 27] By introducing different levels of disorders or defects and by controlling the position of Fermi level, it is expected that TE property can be greatly tuned and optimized.[28, 29] The underlying mechanism is that electronic transport is immune to backscattering by non-magnetic disorders and defects, while phonon transport is not. Thus, the two kinds of transport can be effectively decoupled, realizing the "phonon-glass, electron-crystal" concept and improved TE performance in TIs.[24, 27–29] As the thickness of TI films or the radius of TI nanowires decreases to the order of the localization width of boundary states, a hybridization gap opens at the DP.[30–32] The appearance of a hybridization gap is advantageous for the Seebeck effect but partly destroys the topological protection of the boundary states.[28, 29] Nevertheless, the TI boundary states can still have superior transport ability even with a hybridization gap, leading to an enhanced *ZT*.[33] The theoretical studies under the two conditions (i.e., without and with the hybridization effect) will mainly focus on discussing electronic transport, as factors that affect thermal properties, such as increased boundary scatterings, should be similar as that for other common nanostructures, which has been well established in previous classical articles.[10, 34–36]

The potential of topological states for thermoelectricity in nanostructures also encourages experimental efforts to synthesize high-quality TI nanostructures by various methods such as molecular beam epitaxy (MBE), chemical vapor deposition (CVD) and so on.[37–44] Experimental measurements have also been taken to further investigate the contribution of TI boundary states to thermoelectricity.[45–48]

THEORETICAL CALCULATION

In TIs there exist two types of states, bulk states and boundary states. Both of them have contributions to TE transport. As bulk states and boundary states exhibit distinct band structures and show considerably different transport properties (one is topologically protected, the other is not), a multiple-channel model is adopted to describe TE properties of TIs. TE transport quantities (the electrical conductance and Seebeck coefficient) are denoted as bulk (G_b, S_b), edge (G_e, S_e)/surface (G_s, S_s), and total (G_t, S_t) parts, respectively. They are related by the relations:[2]

$$\text{2D TI} \quad G_t = G_b + G_e \tag{1}$$

$$S_t = (S_b G_b + S_e G_e)/(G_b + G_e) \tag{2}$$

$$\text{3D TI} \quad G_t = (G_b + G_s) \tag{3}$$

$$S_t = (S_b G_b + S_s G_s)/(G_b + G_s) \tag{4}$$

Note that the contributions of edge/surface states show different dependence on geometric sizes (i.e., cross sectional area *A* and transport length *L*) compared to that of bulk states. Thus, the conductance is used instead of the conductivity for properly describing the TE size effect.[28, 29] Based on the multiple-channel model, theoretical studies have been performed under two different conditions, with and without the hybridization effect in boundary states.

Without the hybridization effect—TI boundary states working as superior conducting channels

Improving TE performance requires reducing thermal conductivity while keeping electrical conductivity and Seebeck coefficient in high values.[1] Topologically protected boundary states in TIs working as conducting channels are quite promising for this purpose, as they have lower physical dimension than the bulk states, and also show excellent transport ability due to the absence of backscattering. As a result, by controlling the geometric sizes and introducing disorders and defects, the relative contributions of electrons (including both bulk and boundary states) and phonons can be tuned and TE properties of TIs thus can be improved.[28, 29] The schematic band structure of TIs is depicted in Fig. 2a. Due to the unique band structure, some novel phenomena and important parameters will be discussed in the following parts.

Anomalous Seebeck effects generated by TI boundary states. It is critical to realize sizable Seebeck coefficients by gapless band structures. Usually, the Seebeck effect is weak for metallic materials without opening a band gap, since both electron- and hole-like charge carriers will be thermally excited and have opposite contributions to the Seebeck coefficient, therefore, compensating each other. However, when the Fermi level is located around the bulk band edges, conduction band minimum (CBM) or valence band maximum (VBM), sizable Seebeck values with anomalous signs can be generated by gapless boundary states due to a strong energy dependence in the scattering time caused by the boundary-bulk interactions, as predicted by theoretical calculations.[26–28, 49]

In order to understand the anomalous sign and sizable value of *S* of TI boundary states, some basic knowledge of *S* will be briefly introduced here. The Seebeck effect represents the response of electrons to external temperature gradient. Electronic states below and above the Fermi level show different behaviors, leading to opposite signs of *S*.[2] When the temperature increases, the occupation of electrons gets decrease or increased, depending on whether the energy of electrons is below or above the Fermi level, thus having opposite contributions to *S*. When the charge

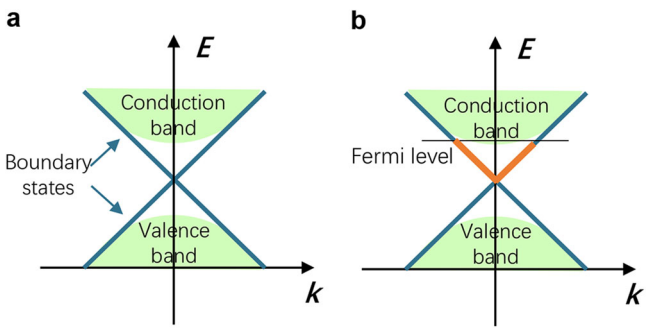

Fig. 2 **a**, **b** Band structures of TIs. The insulator-like bulk bands are in *green* and the metallic boundary states are in *blue*. Boundary states with energies above the Dirac points are mostly unoccupied as displayed in *orange*

carriers above the Fermi level E_F dominate TE transport, S is negative, and otherwise S is positive. Typically S is estimated by using the Sommerfield expansion:[50]

$$S = -\frac{\pi^2 k_B^2 T}{3e}\frac{\partial \ln\left[\tilde{\mathcal{T}}(E)\right]}{\partial E}|_{E=E_F}, \quad (5)$$

which can be derived from the Landauer formula under the conditions of low T and smooth transmission function $\tilde{\mathcal{T}}(E)$. $\tilde{\mathcal{T}}(E)$ contains the information on band structure and scattering, which are described by the distribution of conduction modes $M(E)$ and the mean free path $\lambda(E)$, respectively.[51] The slope of $\tilde{\mathcal{T}}(E)$ at E_F determines the value of S. For diffusive transport, $\tilde{\mathcal{T}}(E)$ is proportional to the product of $M(E)$ and $\lambda(E)$. Generally, there are two mechanisms to enhance S: an increased energy dependence of $M(E)$, for example by introducing a large local variation in the density of states, generating strong Seebeck effect;[10, 13] and an increased energy dependence of $\lambda(E)$.[52]

As to the discussion about the anomalous Seebeck effect in TI boundary states, the underlying reasons are listed as follows. Firstly, S exhibits a sizable value due to the strong energy dependence of $\lambda(E)$, though the band structure of TI boundary states is gapless, which gives a weak energy dependence of $M(E)$. The energy dependence of $\lambda(E)$ or scattering time $\tau(E)$ is usually weak and neglected in most TE studies. However, in TIs the boundary-bulk interactions are able to induce a strong energy dependence of $\lambda(E)$ or $\tau(E)$ when the electron energy is around the bulk band edges,[28, 29] which plays a crucial role in enhancing S of the TI boundary states. Using a 2D TI as an example, when E_F is located around the bulk CBM and above the DP, the charge carriers are expected to be electron-like from Hall measurements. However, for the Seebeck effect, the edge states above E_F are strongly scattered by defects/disorders due to the edge-bulk interactions, while the edge states below E_F (Fig. 2b) and within the bulk band gap are topologically protected against back-scattering. The later has dominated contribution to the Seebeck effect, giving a positive (or hole-like) S. Similarly, we can get a negative S when the Fermi level is placed around the bulk VBM. Benefiting from the edge-bulk interactions, a sizeable S can be obtained without breaking the gapless TI boundary states. Thus TI boundary states can simultaneously have sizable S and superior mobility, advantageous for TE applications.

Fermi level. It is well known that the position of Fermi level (E_F) or chemical potential (μ) of electrons is a critical factor determining transport behaviors of a given TE material.[5, 13, 53] For TIs, E_F not only tunes the transport behavior of each channel (bulk or boundary channel) but also controls their relative contribution to TE transport. In addition, TE transports of bulk and boundary states are optimized with quite different E_F.[49] ZT of the boundary states becomes larger when E_F is outside the bulk band gap, while ZT of the bulk states can be larger when E_F is within the bulk band gap. Moreover, when E_F is within the bulk band gap, carriers on boundary states dominate the TE transport in TI nanostructures; while the bulk states become dominated when E_F is outside the bulk band gap. Therefore, it is expected that a compromise is required to achieve the optimized performance. Calculations show that the optimal E_F for large Seebeck coefficients is near the bulk CBM or VBM as we mentioned in above section, and so is it for the overall TE performance.[26–28, 49] E_F can be tuned by various methods, such as chemical doping and gating voltage,[54–57] to realize the optimal position.

Scattering

Inelastic scattering and effective system size: The intriguing property to suppress backscatterings of charge carriers at non-magnetic impurities and defects makes topologically protected boundary states distinct from ordinary bulk states.[58] However, the topological protection against backscattering is based on the existence of phase coherence, which could be broken once the boundary states undergo inelastic scattering. Therefore, the inelastic mean free path l_{inel} gives an effective system size (L) for quantum transport by boundary states.[49]

Scattering time ratio: As we mentioned previously in "anomalous Seebeck coefficient generated by TI boundary states", Seebeck coefficient is critically related to the energy dependence of mean free path $\lambda(E)$ or scattering time $\tau(E)$. In TIs, the scattering time of boundary states $\tau(E)$ is significantly longer than that of bulk states. More importantly, $\tau(E)$ shows a strong energy dependence. For E within the bulk band gap, boundary states are topologically protected against backscattering, having a large scattering time τ_1; while for E outside the bulk band gap (i.e., overlapping with bulk bands) backscattering is allowed due to the interactions between bulk and boundary states, resulting in a decreased relaxation time τ_2. As a consequence, the dual scattering time model was proposed[25] and adopted in the calculations.[28, 29] Typically τ_1 is much larger than τ_2. The scattering time ratio ($\gamma_\tau = \tau_1/\tau_2$), thus represents discontinuity of the scattering time of the boundary states around the bulk band edges (CBM or VBM). A large discontinuity gives a strong energy dependence of $\tau(E)$, which is favorable for a large S.

Calculations have been made by assuming different values of γ_τ.

$(1)\gamma_\tau = \infty$

Elastic backscatterings generated by non-magnetic impurities and defects are prohibited for 1D edge states of 2D TIs and 1D conduction channels contributed by line dislocations in 3D topological anderson insulators (TAIs),[26, 27, 49, 59] which implies a very large τ_1. Some previous calculations used a simplified way to deal with transport of boundary states by assuming that boundary states only exist within the bulk band gap.[26] The truncation of bands at the bulk band edges, as schematically shown in Fig. 3a, actually assumes $\tau_2 = 0$ and $\gamma_\tau = \infty$. Under this assumption, ZT values of the edge, bulk and total contributions were all calculated as the functions of chemical potential μ at T=1.8 K, showing a dominated contribution of edge state and a total TE enhancement with E_F near the CBM. For 3D TAIs including line dislocations,[59] thermal conductivity is strongly suppressed by the dislocations, while electrical conductivity is maintained as these line dislocations serve as topologically protected 1D conducting channels. The band structure of this system is modeled as a semiconductor with one valence, one conduction band, and one 1D-state

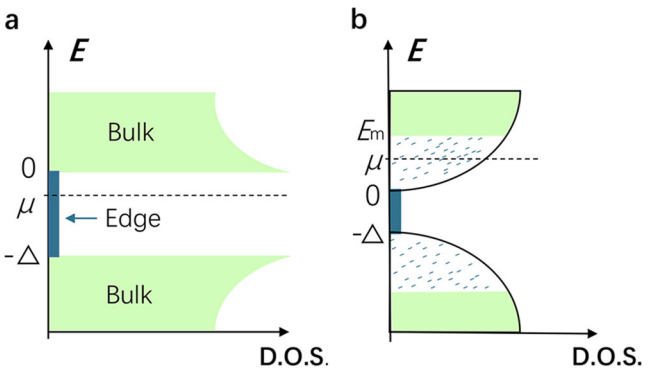

Fig. 3 **a**, **b** Density states used in calculation of ideal 2D TIs and 3D TAIs with line dislocations. Bulk states are denoted in *green*, and conducting channels are in *blue*. (**a** adapted from ref. 49 with permission, Copyright 2010 American Physical Society) (**b** adapted with from ref. 59 with permission, Copyright 2010 American Institute of Physics)

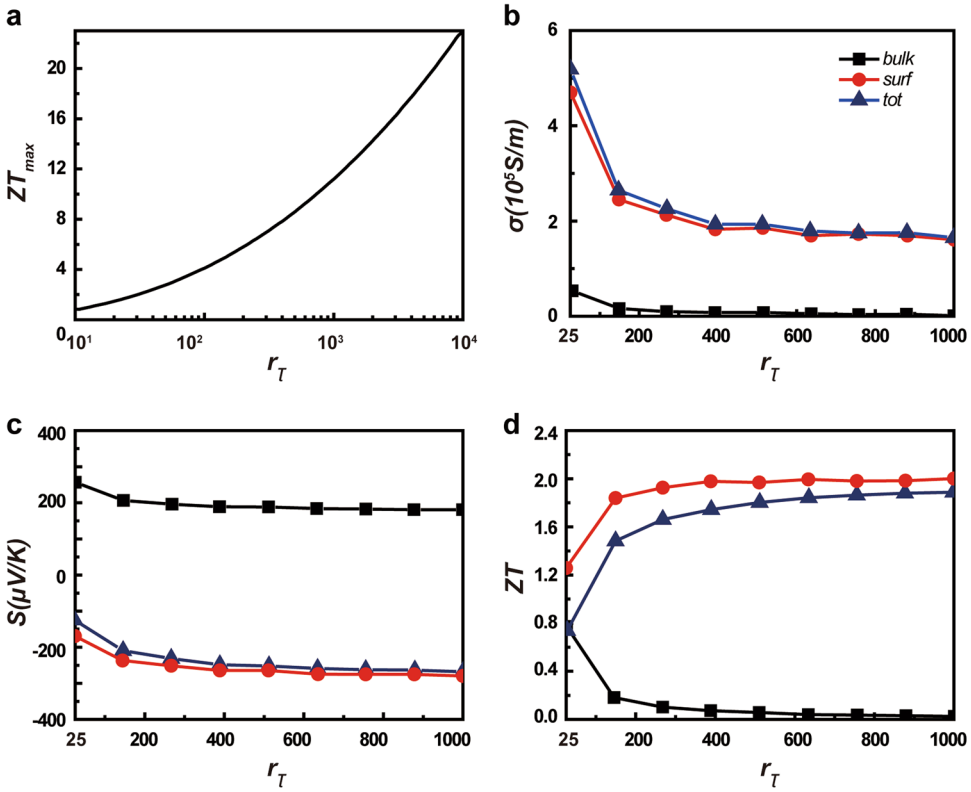

Fig. 4 **a** The maximum possible *ZT* of 2D TIs, ZT_{max}, as a function of the scattering-time ratio γ_τ. **b**, **c**, and **d** electrical conductivity σ, Seebeck coefficient *S*, and figure of merit *ZT* of the p-type 3-QL Bi_2Te_3 film as a function of the relaxation time ratio γ_τ. Contributions from the surface and bulk states are also shown in **b**, **c**, and **d** (**a** adapted with permission from ref. 28 Copyright 2014 by the American Physical Society. **b**-**d** adapted from ref. 29 with permission of The Royal Society of Chemistry

corresponding to perfectly conducting line dislocations (in general, one 1D-state per each dislocation), as shown in Fig. 3b. The bulk states near the edges of the band are localized with a mobility edge at E_m; this Anderson bulk localization is due to the high density of dislocations or induced by doping with non-magnetic impurities. The excellent transport of the 1D channels dominates the total transport, when the chemical potential is restricted within the bulk band gap, $-\Delta < \mu < 0$, or close to the mobility edge E_m. The largest total value can be obtained when the chemical potential is slightly above E_m.

$(II)\gamma_\tau \neq \infty$

Some other calculations have been made for more realistic conditions, based on the intrinsic properties of boundary states. A finite scattering ratio is introduced, which is a crucial factor affecting the TE performance.[28, 29] The scattering time ratio can be tuned by introducing non-magnetic defects or disorders into the system.[52]

In order to demonstrate the influence of scattering time ratio on the TE performance of a 2D TI, the upper limit of *ZT* (ZT_{max}) was discussed by neglecting the lattice thermal conductance in a previous work,[28] showing that ZT_{max} increases monotonically with increasing γ_τ (Fig. 4a). The contribution of lattice thermal conductance was also discussed by considering a finite mean free path of phonons. The mean free path ratio between phonons and boundary electrons could be minimized by introducing defects or disorders into the system, which improves TE performance.[28]

For nanostructures of 3D TIs, Bi_2Te_3 thin films for example,[29] γ_τ also serves as an important factor for TE performance. Figure 4b, c, and d plot the transport coefficients and *ZT* value of the P-type 3-quintuple layer (QL) film at room temperature with optimized carrier concentration *n* as a function of γ_τ. The contributions from the bulk and surface states are also shown in Fig. 4b, c, and d, respectively. As we have shown, *ZT* value is dominated by surface contributions. Also the value increases steadily with the increasing γ_τ. Similar findings can be obtained for the N-type 3-QL film and thicker TI films. In short, here the 3D TIs with topological surface states are capable to realize an enhancement in TE performance by increasing the relaxation time ratio between the surface and bulk states via introducing disorders and impurities.

Geometry size dependence. In TI systems when boundary states are topologically protected to coexist with bulk states, *ZT* is no longer an intrinsic property for nanostructured TIs, but is strongly affected by the geometric size. The geometric size not only determines whether or not the hybridization of boundary states happens, but also tunes the relative contribution of boundary and bulk states to TE transport. A previous work found that *ZT* of 2D TIs could be tuned by varying the transport length and ribbon width.[28] When increasing the transport length and decreasing the ribbon width, the contribution of edge states will be enhanced, leading to an improved *ZT*. The contribution of edge states is maximized by setting the transport length larger than the inelastic scattering length l_{inel} and the ribbon width about two times the localization width of edge states. This is also the optimized geometry for total TE performance, achieving the maximal *ZT* ($ZT > 6$). The concept was generalized to 3D TIs in the following work, which made a calculation in Bi_2Te_3 thin films, showing the highest *ZT* value ($ZT \sim 2$) achieved at the critical thickness of three QLs, where the topologically non-trivial surface states start to appear.[29] As the thickness becomes larger, the contribution of bulk weights more and the lattice thermal conductance increases, leading to a decreased *ZT* value.

With the hybridization effect —opening a Dirac gap

When the size of a TI nanostructure scales down to the order of the localization width of boundary states, a hybridization gap induced by coupling between boundary states from opposite sides will open at the DP,[30–32, 60, 61] whose influence on TE performance will be discussed.

Subband gap versus thickness. A thin film of 3D TI is considered with a finite thickness d, as shown in Fig. 5a. The surface and interior regions are denoted by blue and green colors, respectively. When the thickness d decreases to a certain degree (~ 1–10 nm), a subband gap ΔE_s shows up induced by hybridization between the top and bottom surface states, as shown in Fig. 5b.

Relationships between the thickness d and the bulk as well as hybridization gaps in Bi_2Te_3, Sb_2Te_3, and Bi_2Se_3 thin films have been theoretically studied. Calculations show that the bulk gap ΔE_b increases with decreasing film thickness d.[62] The hybridization gap ΔE_s opens at $d < 6$ nm for Bi_2Se_3, $d < 2$ nm for Bi_2Te_3, and $d < 4$ nm for Sb_2Te_3 and also displays an increasing tendency with decreasing d, as theoretically and experimentally proved.[38, 39, 62, 63]

Calculations of individual TI nanostructures. Ghaemi et al.[33] performed theoretical calculations on TI thin films with hybridization-induced band gaps. Bi_2Te_3 thin films for example is found to have a remarkably increased ZT value of surface states at low temperature in a relatively large range of chemical potential. The enhancement in TE performance of surface states also leads to an increased total ZT, as the surface contribution plays a dominant role when the chemical potential is within the bulk band gap. It should be noted that the bulk contribution of Bi_2Te_3 is assumed to be a constant value at a given temperature in this study. While the chemical potential dependence of bulk properties can be neglected at low temperature when the surface contribution is dominant, this simplification doesn't make sense at room or higher temperature. Contributions of bulk states are calculated explicitly instead of being assigned in some other calculations.[29, 62, 64] Osterhage et al.[62] calculated the surface, bulk and total contributions of Bi_2Te_3, Sb_2Te_3, Bi_2Se_3 thin films, and found that the total ZT was actually enhanced compared to the calculated ZT of the bulk. However, a significant enhancement ($ZT > 2$) is difficult to achieve, since contributions of bulk and surface are optimized at different Fermi levels. An enhancement of total ZT was also calculated by Liang et al.[29] in 1- and 2 -QL Bi_2Te_3 films compared with bulk Bi_2Te_3 in its pristine form ($ZT = 0.4$). In all these calculations, the total ZT is found to monotonically increase with decreasing film thickness, due to the increasingly important hybridization effect.

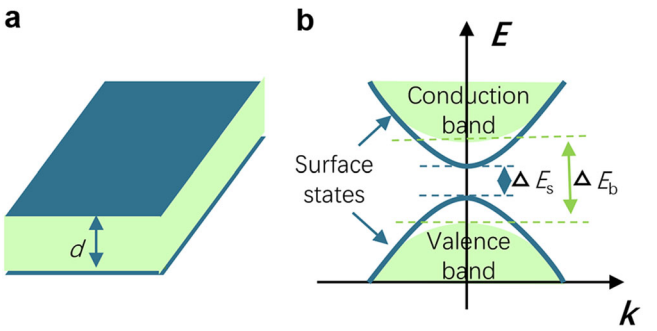

Fig. 5 **a** Sketch of a topological insulator film with two parallel transport channels: bulk (*green*) and surface (*blue*). **b** Schematic diagram of a thin TI film with surface hybridization. *Solid bands* (*green*) are separated by an energy gap ΔE_b and a subbgap gap ΔE_s (*blue solid curves* in **b**) opens around the Dirac point, induced by hybridization of TI states of the two opposed faces

Calculations in designed porous structures. Just like line dislocations in 3D TAIs as connecting channels, high density of holes (pores) can be introduced to a 3D TI to create surface states. High density of hole surfaces significantly suppresses the phonon thermal conductivity, and meanwhile cause hybridization among these surface states, inducing a controllable Dirac subband gap to further increase ZT.[65] This calculation is not limited to periodic holy structures, porous TIs with random sizes and location of pores can also be used to achieve a high ZT.

EXPERIMENTAL TRIALS

Above theoretical discussions indicate the potentials that TIs possess in TE performance, and also offer a guidance for related experimental trials. Firstly, nano-engineering is of great importance, for either increasing contributions of TI boundary states or opening hybridization band gaps. Secondly, the Fermi level with respect to the bulk bands and the DP is also crucial, as it determines the relative contribution of bulk and boundary states to TE transport in TIs. Therefore, well preparation of TI nanostructures is the first and critical step in experiments. Here, we will first give a brief review on recent progress in preparing TI nanostructures, since several excellent review articles have already detailed different approaches in synthesis of various TI nanostructures.[41, 66] After that, TE measurements on TI nanostructures will be discussed.

Approaches to prepare TI nanostructures

Several kinds of TI materials with promising TE properties have been found: group V–VI semiconductors (Bi_2Te_3, Sb_2Te_3, Bi_2Se_3, and their derivatives), SnTe, PbSnTe, etc. Here, we will give a brief review on experimental methods of preparing their high-quality nanostructured counterparts, and different traits of each method will also be covered as summarized in Table 1. In general, these preparing methods can be divided into two broad categories: top-down fabrication methods which utilize bulk sources to produce nanostructures, such us mechanical or chemical exfoliation from bulk crystals, and bottom-up methods which make nanostructures assembled from atomic or molecular scale, including epitaxy, vapor deposition and solution synthesis. With these methods, nanostructures of TIs in variant morphologies can be obtained, including thin films, nanoplates, nanosheets, nanowires, and nanoribbons. For the preparation of TI thin films, MBE takes advantages for its high crystal quality and precise control of film thickness down to atomic layers, while has disadvantages of high cost and low efficiency.[37–40] On the contrary, exfoliation,[67, 68] especially mechanical exfoliation, is another way to get high-quality nanosheets of layered TIs, which operates conveniently but with poor controllability and size limitation. CVD and solvothermal synthesis can produce TI nanoplates in high yield with relatively high quality and some degree of controllability at the same time.[42, 43, 69–77] It is to be noted that CVD has an advantage over solvothermal synthesis in sample quality for its relative clean reaction system. CVD and solvothermal synthesis play more significant roles in preparing 1D TI materials such as nanowires, nanoribbons, and nanotubes.[72, 73, 75–77]

Thanks to tremendous progress in recent years, high quality of TI nanostructures with considerable surface contributions is realized and verified by various measurements. Metallic surface band structures in angle-resolved photoemission spectroscopy (ARPES), Landau quantizations, Aharonov-Bohm (AB) oscillation and Shubnikov-de Haas oscillations have been observed in TI thin films, nanoribbons or nanowires,[23, 37–39, 42, 78–80] and hybridization of surface states has also been observed in ultra-thin TI films.[38] These experimental results demonstrate the excellent sample quality and reveal significant surface contributions.

Table 1. Summary and comparison of various synthesis methods

Categories	Methods		Advantages	Disadvantages	Example materials	Morphology
Top-down	Exfoliation	Mechanical exfoliation	Low cost, easy to operate and able to get clean and pristine samples	Poor controllability, low yield, small sized, and irregular shaped samples	Layer crystal: Bi_2Te_3, Sb_2Te_3, Bi_2Se_3, etc	Nanosheets
		Chemical exfoliation	Low cost and easy to operate	Small sized and irregular shaped samples		Nanosheets
Bottom-up	Chemical vapor deposition (CVD)		Relatively high quality and mass produced	Not well-controlled in shape and accurate stoichiometry	Bi_2Te_3, Sb_2Te_3, Bi_2Se_3, SnTe, PbSnTe, etc	Nanoplates, Nanoribbons, Nanowires
	Molecular beam epitaxy (MBE)		High quality and precise control of film thickness to atomic layer	Low growth speed and high cost	Bi_2Te_3, Sb_2Te_3, Bi_2Se_3, etc	Ultra-thin films
	Solvothermal synthesis		Easy to implement doping and mass production	Impurities residual	Bi_2Te_3, Sb_2Te_3, Bi_2Se_3, etc	Nanoplates, nanoribbons, Nanowires

Contributions of surface states in TE transport of nano-engineered TIs

Individual TI nanostructures. Although theoretical studies and synthesis technologies lay solid foundation, not so many experimental studies on TE transport of individual TI nanostructures have been reported mainly due to challenges in clean transfer and precise TE measurement. TI nanowires produced by vapor deposition and TI nanosheets produced by mechanical exfoliation have been mostly used in these studies.[46, 81–84]

TE performance of individual TI nanostructures compared with their counterparts have been reported in some experimental works. TE related values (electrical conductivity, Seebeck coefficient, thermal conductivity, and *ZT* value) of some nanostructures (Bi_2Te_3 thin film,[82] Bi_2Se_3 nanoribbon,[81] Sb_2Te_3 nanowire,[46] $Bi_{1.5}Sb_{0.5}Te_{1.7}Se_{1.3}$ nanowires,[85] SnTe nanowire,[84] and PbSnTe nanowire[83]) normalized by respective values of their bulk counterparts at room temperature are summarized in Fig. 6. Suppressed thermal conductivity is observed in most nanostructures, attributing to enhanced boundary scattering, while properties related to electrical transport exhibit diverse behaviors. So far it is difficult to build the relations between diverse TE performances and topological nature for several reasons. Firstly, some of the samples are highly doped in the bulk, decreasing the relative contribution of topological surface states. Secondly, diverse electrical transport behaviors can also be attributed to band structure changing during nano-engineering. Therefore, it is difficult to reveal the contributions of topological states of a TI nanostructure just from the *ZT* value of the given TI nano-sample.

Still a few works provide some indications of contributions that topological surface states make in TE transport through a series of measurements and analysis. Conjoint measurement of TE and magnetotransport perhaps offers more information. Approximately 13 times enhancement of *ZT* value has been observed in $Bi_{1.5}Sb_{0.5}Te_{1.7}Se_{1.3}$ (BSTS) nanowires ($ZT = 0.36$) compared with the bulk specimen ($ZT = 0.028$), primarily owing to an order of magnitude increase in the electrical conductivity and a large Seebeck coefficient.[85] Electrical transport behavior under 300 K along with the notable deviation in resistance to a 3D variable-range hopping model (3D VRH) fitting indicates the existence of a parallel metallic conduction of surface states. In addition, results of magnetotransport test further manifest that E_F lies within the bulk band gap. The results of TE and magnetotransport prove the existence even the domination of surface-states transport in BSTS nanowires, which possess low carrier density and high mobility to generate large electrical conductivities and Seebeck coefficients. The experiment demonstrates the possibility of using TI surface states to improve *ZT*, although the relative contribution of surface states is not quantitatively determined. The key feature of this experiment is that the chemical potential of the as grown TI materials is located within the bulk gap, enhancing the relative contribution of surface-state transport. Moreover, rough boundary of TI nanowires could significantly scatter phonons and bulk states while have much less influence on the transport of TI surface states, thus keeping high electrical conductivities in nanowires. Contributions of topological surface states in TE transport can also be studied by tuning the band structure or E_F. A previous experiment found that by tuning the chemical composition *x* of $(Bi_{1-x}Sb_x)_2Te_3$ TI thin films, band structure and Fermi level would systematically change as confirmed by ARPES measurements, which has profound influence on TE properties.[48] Unexpectedly, an electron-like Hall effect and a hole-like Seebeck effect appear simultaneously in a TI thin film for all the experiment temperatures (under room temperature). This sign anomaly is well explained by the two channel model, in which the Seebeck effect is dominated by the bulk-state channel that shows a larger Seebeck coefficient, while the Hall effect is dominated by the gapless surface-state channel that gives a larger mobility due to the

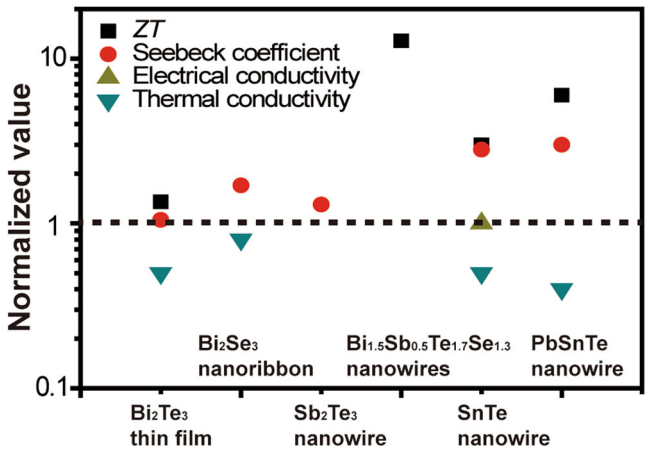

Fig. 6 TE related values (electrical conductivity, Seebeck coefficient, thermal conductivity and *ZT* value) of various nanostructures (Bi_2Te_3 thin film,[82] Bi_2Se_3 nanoribbon,[81] Sb_2Te_3 nanowire,[46] $Bi_{1.5}Sb_{0.5}Te_{1.7}Se_{1.3}$ nanowires,[85] SnTe nanowire,[84] and PbSnTe nanowire[83]) normalized by respective values of their bulk counterparts at room temperature

topological protection. Ternary TI $(Bi_{1-x}Sb_x)_2Te_3$ nanowires were studied by changing the Bi-Sb ratios.[86] $(Bi_{1-x}Sb_x)_2Te_3$ nanowires exhibit an abrupt sign change from positive to negative values in Seebeck coefficients and a low electrical conductivity with the Sb concentration from $x = 1$ to $x = 0$. The transport behavior differs noticeably from that for single-crystalline bulk sample, which is consistent with the theoretical calculations based on the two channel model, suggesting that TE properties of $(Bi_{1-x}Sb_x)_2Te_3$ NWs are not only derived from their bulk counterparts, but also critically from surface state contribution. Moreover, in TI thin films, the relative contribution of surface states to TE transport could be systematically controlled by varying the film thickness. This is demonstrated by a recent experiment on the epitaxial Bi_2Se_3 TI thin films of varied thicknesses,[47] which shows that the metallic TI surface states become more and more important in thinner films, leading to decreased Seebeck coefficients and power factors. Further enhancement of TE performance can be expected by optimizing E_F and introducing disorders or defects into the samples for utilizing the advantage of topological protection.

TI nanocomposites. It's an even more challenging task to clearly see whether surface states contribute in TE transport of TI nanocomposites. In recent years, improved TE performances of TI nanocomposites compared with bulk counterparts have often been reported. However, they are mostly attributed to suppression of phonon transportation or filtering of low-energy electrons.[7, 87] Sun et al.[88] found some evidence of the surface contributions through a series of measurements and analysis. The electron mobility μ in Bi_2Se_3 nanocomposites produced by milling and sintering is found to increase by 50 times at 300 K, when the grain size decreases from microns to ~80 nm in thickness. In contrast, the electron mobility in conventional semiconductors or conductors always decreases with decreasing grain sizes due to enhanced carrier scattering by increased grain boundaries. Hence, the anomalous mobility enhancement here can be reasonably attributed to topological surface states in Bi_2Se_3 nanoparticles. As grain size decreases, the volume fraction of the gapless conducting surfaces increases, providing superior transporting channels and enhancing overall mobility. However, it's common to observe a decreased electrical conductivity in TI nanostructures. The underlying role of TI surface states remains unclear until now and is awaiting to be explored in the future.

CONCLUSION AND OUTLOOK

In this review, we discussed the potential impact of TI boundary states on thermoelectricity from both theoretical and experimental points of view. Past several years have witnessed encouraging progress, especially in theoretical studies. Enhanced TE performances by utilizing TI boundary states have been predicted in TI nanostructures under specific conditions, with and without the hybridization effect in boundary states. On experimental side, while various methods have also been developed to prepare high-quality TI nanostructures in recent years, enhanced *ZT* as predicted by theoretical studies has rarely been observed in experiments, possibly due to a few reasons. Firstly, precise TE measurement of nanostructures is still a challenging task. Secondly, a fine tuning of Fermi level is of key importance to optimize TE performance of TI nanostructures, which, however, has been rarely demonstrated experimentally. Thirdly, for some high-quality TI thin films by MBE, without intendedly introducing disorders and defects into the materials, the advantage of high mobility of TI boundary states due to the topological protection cannot be fully manifested. The last but not least, nano-engineering not only magnifies contributions of boundary states, but also impact the transport of bulk states, which makes it quite difficult to separate the boundary contributions from other factors. Therefore, it is clear that more experimental effort is required to clearly figure out the underlying relations between TE performance and topological nature and to fully utilize the advantages of TI boundary states for improving *ZT* values.

Based on current progress and existing challenges, there remains much work awaiting to be done in the future. Most of the previous theoretical works have focused on TE transport of individual TI nanostructure, while complex structures and systems such as superlattices or nanocomposites with intriguing surface/interface properties and wide practical use are seldom involved. Moreover, various ways of controlling TI boundary states, for instance, by topological phase transition (e.g., alloying, applying electric field, or strain) or by symmetry breaking (e.g., applying magnetic field to break time reversal symmetry), remain to be explored for designing new TE devices. Experimentally, to optimize TE performance, a fine tuning of Fermi level is necessary but has been rarely demonstrated in most of TI nanostructures. Also to manifest the advantage of high mobility of TI boundary states while minimizing the thermal conductance, it is desirable to develop new techniques to further reduce the geometry size of TI nanostructures and to introduce disorders and defects into the TI materials. In addition, more systematic measurements including TE transport and magnetotransport are needed to clarify effects of topological boundary states for TE applications. Moreover, various types of TI nanostructures should be investigated, to reveal more convincing and general conclusions on the relations between TE properties and topological nature in Tis, and ultimately leading to design and fabrication of high-performance TI nanocomposites for practical TE applications at large scales.

With exciting progress on-going in both TIs and thermoelectrics, it is clear that there are tremendous opportunities existing at the intersection of these two rapidly evolving fields. Therefore, it is expected that future progress will not only advance our understanding on TE properties of TI boundary states, but also provide new insights and innovated ways to design and develop high-performance TE devices.

ACKNOWLEDGEMENTS

This work is jointly supported by the National Key Research and Development Program of China (No. 2017YFA0205700) and the State Key Program for Basic Research of China (No. 2015CB659300), National Natural Science Foundation of China (Nos. 11621091, 11574143), Natural Science Foundation of Jiangsu Province (Nos. BK20150056), the Project Funded by the Priority Academic Program Development of Jiangsu Higher Education Institutions (PAPD) and the Fundamental Research Funds

for the Central Universities (Nos. 021314380068, 021314380089, 021314380091). Y.X. acknowledges support from Tsinghua University Initiative Scientific Research Program and the National Thousand-Young-Talents Program.

ADDITIONAL INFORMATION

Competing interests: The authors declare no competing financial interest.

Publisher's note: Springer Nature remains neutral with regard to jurisdictional claims in published maps and institutional affiliations.

REFERENCES

1. Rowe, D. M. (eds) *CRC Handbook of Termoelectrics*. (CRC press, 1995).
2. Goldsmid, H. J. *Introduction to Thermoelectricity*. (Springer press, 2009).
3. Rowe, D. M. (eds). CRC *Handbook of Termoelectrics: Macro to Nano*. (CRC press, 2005).
4. Goldsmid, H. J. *Thermoelectric Refrigeration*. (Plenum Press, 1964).
5. Snyder, G. J. & Toberer, E. S. Complex thermoelectric materials. *Nat. Mater.* **7**, 105–114 (2008).
6. Sootsman, J. R., Chung, D. Y. & Kanatzidis, M. G. New and old concepts in thermoelectric materials. *Angew. Chem. Int. Ed. Engl.* **48**, 8616–8639 (2009).
7. Poudel, B. et al. High-thermoelectric performance of nanostructured bismuth antimony telluride bulk alloys. *Science* **320**, 634–638 (2008).
8. Szczech, J. R., Higgins, J. M. & Jin, S. Enhancement of the thermoelectric properties in nanoscale and nanostructured materials. *J. Mater. Chem.* **21**, 4037–4055 (2011).
9. Pei, Y. et al. Convergence of electronic bands for high performance bulk thermoelectrics. *Nature* **473**, 66–69 (2011).
10. Dresselhaus, M. S. et al. New directions for low-dimensional thermoelectric materials. *Adv. Mater.* **19**, 1043–1053 (2007).
11. Mohanraman, R. et al. Engineering nanostructural routes for enhancing thermoelectric performance: bulk to nanoscale. *Front. Chem.* **3**, 1–9 (2015).
12. Heremans, J. P. et al. Enhancement of thermoelectric efficiency in PbTe by distortion of the electronic density of states. *Science* **321**, 554–557 (2008).
13. Pei, Y., Wang, H. & Snyder, G. J. Band engineering of thermoelectric materials. *Adv. Mater.* **24**, 6125–6135 (2012).
14. Biswas, K. et al. High-performance bulk thermoelectrics with all-scale hierarchical architectures. *Nature* **489**, 414–418 (2012).
15. Zhao, L. D., Dravid, V. P. & Kanatzidis, M. G. The panoscopic approach to high performance thermoelectrics. *Energy Environ. Sci.* **7**, 251–268 (2014).
16. Zheng, Y. et al. Mechanically robust BiSbTe alloys with superior thermoelectric performance: a case study of stable hierarchical nanostructured thermoelectric materials. *Adv. Energy Mater.* **5**, 1401391 (2015).
17. Moore, J. E. The birth of topological insulators. *Nature* **464**, 194–198 (2010).
18. Kong, D. & Cui, Y. Opportunities in chemistry and materials science for topological insulators and their nanostructures. *Nat. Chem.* **3**, 845–849 (2011).
19. Zhang, H. et al. Topological insulators in Bi_2Se_3, Bi_2Te_3 and Sb_2Te_3 with a single Dirac cone on the surface. *Nat. Phys.* **5**, 438–442 (2009).
20. Hsieh, D. et al. Observation of time-reversal-protected single-dirac-cone topological-insulator states in Bi_2Te_3 and Sb_2Te_3. *Phys. Rev. Lett.* **103**, 146401 (2009).
21. Hsieh, T. H. et al. Topological crystalline insulators in the SnTe material class. *Nat . Commun.* **3**, 982 (2012).
22. Chen, Y. L. et al. Experimental realization of a three-dimensional topological insulator, Bi2Te3. *Science* **325**, 178–181 (2009).
23. Zhang, J. et al. Band structure engineering in $(Bi_{1-x}Sb_x)_2Te_3$ ternary topological insulators. *Nat. Commun.* **2**, 574 (2011).
24. Müchler, L., Casper, F., Yan, B., Chadov, S. & Felser, C. Topological insulators and thermoelectric materials. *Phys. Status Solidi - R* **7**, 91–100 (2013).
25. Xu, Y. Thermoelectric effects and topological insulators. *Chin. Phys. B* **25**, 117309 (2016).
26. Murakami, S., Takahashi, R., Tretiakov, O. A., Abanov, A. & Sinova, J. Thermoelectric transport of perfectly conducting channels in two- and three-dimensional topological insulators. *J. Phys.: Conf. Ser.* **334**, 012013 (2011).
27. Takahashi, R. & Murakami, S. Thermoelectric transport in topological insulators. *Semicond. Sci. Technol.* **27**, 124005 (2012).
28. Xu, Y., Gan, Z. & Zhang, S. C. Enhanced thermoelectric performance and anomalous seebeck effects in topological insulators. *Phys. Rev. Lett.* **112**, 226801 (2014).
29. Liang, J., Cheng, L., Zhang, J., Liu, H. & Zhang, Z. Maximizing the thermoelectric performance of topological insulator Bi_2Te_3 films in the few-quintuple layer regime. *Nanoscale* **8**, 8855–8862 (2016).
30. Linder, J., Yokoyama, T. & Sudbø, A. Anomalous finite size effects on surface states in the topological insulator Bi_2Se_3. *Phys. Rev. B* **80**, 205401 (2009).
31. Liu, C. X. et al. Oscillatory crossover from two-dimensional to three-dimensional topological insulators. *Phys. Rev. B* **81**, 041307 (2010).
32. Lu, H. Z., Shan, W. Y., Yao, W., Niu, Q. & Shen, S. Q. Massive Dirac fermions and spin physics in an ultrathin film of topological insulator. *Phys. Rev. B* **81**, 115407 (2010).
33. Ghaemi, P., Mong, R. S. & Moore, J. E. In-plane transport and enhanced thermoelectric performance in thin films of the topological insulators Bi_2Te_3 and Bi_2Se_3. *Phys. Rev. Lett.* **105**, 166603 (2010).
34. Cahill, D. G. et al. Nanoscale thermal transport. *J. Appl. Phys.* **93**, 793–818 (2003).
35. Heremans, J. P., Dresselhaus, M. S., Bell, L. E. & Morelli, D. T. When thermoelectrics reached the nanoscale. *Nat. Nanotechnol.***8**, 471–473 (2013).
36. Minnich, A. J., Dresselhaus, M. S., Ren, Z. F. & Chen, G. Bulk nanostructured thermoelectric materials: current research and future prospects. *Energy Environ. Sci.* **2**, 466–479 (2009).
37. Chen, X., Ma, X. C., He, K., Jia, J. F. & Xue, Q. K. Molecular beam epitaxial growth of topological insulators. *Adv. Mater.* **23**, 1162–1165 (2011).
38. Li, Y. Y. et al. Intrinsic topological insulator Bi_2Te_3 thin films on Si and their thickness limit. *Adv. Mater.* **22**, 4002–4007 (2010).
39. Jiang, Y. et al. Landau quantization and the thickness limit of topological insulator thin films of Sb_2Te_3. *Phys. Rev. Lett.* **108**, 016401 (2012).
40. Zhang, T. et al. Experimental demonstration of topological surface states protected by time-reversal symmetry. *Phys. Rev. Lett.* **103**, 266803 (2009).
41. Shen, J. & Cha, J. J. Topological crystalline insulator nanostructures. *Nanoscale* **6**, 14133–14140 (2014).
42. Peng, H. et al. Aharonov-Bohm interference in topological insulator nanoribbons. *Nat. Mater.* **9**, 225–229 (2010).
43. Kong, D. et al. Topological insulator nanowires and nanoribbons. *Nano Lett.* **10**, 329–333 (2010).
44. He, L., Kou, X. & Wang, K. L. Review of 3D topological insulator thin-film growth by molecular beam epitaxy and potential applications. *Phys. Status Solidi - R* **7**, 50–63 (2013).
45. Mavrokefalos, A. et al. Thermoelectric and structural characterizations of individual electrodeposited bismuth telluride nanowires. *J. Appl. Phys.* **105**, 104318 (2009).
46. Zuev, Y. M., Lee, J. S., Galloy, C., Park, H. & Kim, P. Diameter dependence of the transport properties of antimony telluride nanowires. *Nano. Lett.* **10**, 3037–3040 (2010).
47. Guo, M. et al. Tuning thermoelectricity in a Bi_2Se_3 topological insulator via varied film thickness. *New J. Phys.* **18**, 015008 (2016).
48. Zhang, J. et al. Disentangling the magnetoelectric and thermoelectric transport in topological insulator thin films. *Phys. Rev. B* **91**, 075431 (2015).
49. Takahashi, R. & Murakami, S. Thermoelectric transport in perfectly conducting channels in quantum spin Hall systems. *Phys. Rev. B* **81**, 161302 (2010).
50. Paulsson, M. & Datta, S. Thermoelectric effect in molecular electronics. *Phys. Rev. B* **67**, 241403 (2003).
51. Mahan, G. D. & Sofo, J. O. The best thermoelectric. *Proc. Natl Acad. Sci. USA* **93**, 7346–7349 (1996).
52. Dyck, J. S. et al. Thermoelectric properties of the n-type filled skutterudite $Ba_{0.3}Co_4Sb_{12}$ doped with Ni. *J. Appl. Phys.* **91**, 3698–3705 (2002).
53. Ioffe, A. F. *Semiconductor Thermoelements and Thermoelectric Cooling*. (Infosearch press, 1956).
54. Gooth, J., Hamdou, B., Dorn, A., Zierold, R. & Nielsch, K. Resolving the Dirac cone on the surface of Bi2Te3 topological insulator nanowires by field-effect measurements. *Appl. Phys. Lett.* **104**, 243115 (2014).
55. Saito, Y. et al. Gate-tuned thermoelectric power in black phosphorus. *Nano Lett.* **16**, 4819–4824 (2016).
56. Wang, Y. et al. Gate-controlled surface conduction in Na-doped Bi2Te3 topological insulator nanoplates. *Nano Lett.* **12**, 1170–1175 (2012).
57. Yu, X. et al. Separation of top and bottom surface conduction in Bi2Te3 thin films. *Nanotechnology* **24**, 015705 (2013).
58. Hsieh, D. et al. A topological Dirac insulator in a quantum spin Hall phase. *Nature* **452**, 970–974 (2008).
59. Tretiakov, O. A., Abanov, A., Murakami, S. & Sinova, J. Large thermoelectric figure of merit for three-dimensional topological Anderson insulators via line dislocation engineering. *Appl. Phys. Lett.* **97**, 073108 (2010).
60. Gooth, J. et al. Thermoelectric performance of classical topological insulator nanowires. *Semicond. Sci. Technol.* **30**, 01501 (2015).
61. Cook, A. & Franz, M. Majorana fermions in a topological-insulator nanowire proximity-coupled to ans-wave superconductor. *Phys. Rev. B* **84**, 201105 (2011).
62. Osterhage, H. et al. Thermoelectric properties of topological insulator Bi_2Te_3, Sb_2Te_3, and Bi_2Se_3 thin film quantum wells. *Appl. Phys. Lett.* **105**, 123117 (2014).

63. Yazyev, O. V., Moore, J. E. & Louie, S. G. Spin polarization and transport of surface states in the topological insulators Bi_2Se_3 and Bi_2Te_3 from first principles. *Phys. Rev. Lett.* **105**, 266806 (2010).
64. Li, L. L. & Xu, W. Thermoelectric transport by surface states in Bi_2Se_3-based topological insulator thin films. *Chin. Phys. Lett.* **32**, 047304 (2015).
65. Tretiakov, O. A. & Jairo Sinova, A. A. Holey topological thermoelectrics. *Appl. Phys. Lett.* **99**, 113110–11311 (2011).
66. Guo, Y., Liu, Z. & Peng, H. A roadmap for controlled production of topological insulator nanostructures and thin films. *Small* **11**, 3290–3305 (2015).
67. Coleman, J. N. et al. Two-dimensional nanosheets produced by liquid exfoliation of layered materials. *Science* **331**, 568–571 (2011).
68. Shahil, K. M. F., Hossain, M. Z., Goyal, V. & Balandin, A. A. Micro-Raman spectroscopy of mechanically exfoliated few-quintuple layers of Bi_2Te_3, Bi_2Se_3, and Sb_2Te_3 materials. *J. Appl. Phys.* **111**, 054305 (2012).
69. Alegria, L. D. et al. Structural and electrical characterization of Bi_2Se_3 nanostructures grown by metal-organic chemical vapor deposition. *Nano Lett.* **12**, 4711–4714 (2012).
70. Brom, J. E. et al. Structural and electrical properties of epitaxial Bi_2Se_3 thin films grown by hybrid physical-chemical vapor deposition. *Appl. Phys. Lett.* **100**, 162110 (2012).
71. Cho, S., Butch, N. P., Paglione, J. & Fuhrer, M. S. Insulating behavior in ultrathin bismuth selenide field effect transistors. *Nano Lett.* **11**, 1925–1927 (2011).
72. Fang, L. et al. Catalyst-free growth of millimeter-long topological insulator Bi_2Se_3 nanoribbons and the observation of the pi-Berry phase. *Nano Lett.* **12**, 6164–6169 (2012).
73. Safdar, M. et al. Topological surface transport properties of single-crystalline SnTe nanowire. *Nano Lett.* **13**, 5344–5349 (2013).
74. Wang, W., Poudel, B., Yan, J., Wang, D. Z. & Ren, Z. F. High-yield synthesis of single-crystalline antimony telluride hexagonal nanoplates using a solvothermal approach. *J. Am. Chem. Soc.* **127**, 13792–11379 (2005).
75. Batabyal, S. K., Basu, C., Das, A. R. & Sanyal, G. S. Solvothermal synthesis of bismuth selenide nanotubes. *Mater. Lett.* **60**, 2582–2585 (2006).
76. Deng, Y. et al. Fabrication of bismuth telluride nanotubes via a simple solvothermal process. *Solid State Commun.* **138**, 111–113 (2006).
77. Zhu, H. T. et al. Tri-wing bismuth telluride nanoribbons with quasi-periodic rough surfaces. *J. Mater. Chem.* **21**, 12375 (2011).
78. He, K. et al. Crossover of the three-dimensional topological insulator Bi_2Se_3 to the two-dimensional limit. *Nat. Phys.* **6**, 584–588 (2010).
79. Tang, H., Liang, D., Qiu, R. & Gao, X. Two-dimensional transport-induced linear magneto-resistance in topological insulator Bi2Se3 nanoribbons. *ACS Nano* **5**, 7510–7516 (2011).
80. Safaei, S., Kacman, P. & Buczko, R. Topological crystalline insulator (Pb,Sn)Te: surface states and their spin polarization. *Phys. Rev. B* **88**, 045305 (2013).
81. Tang, H. et al. Thermoelectric characterization of individual bismuth selenide topological insulator nanoribbons. *Nanoscale* **7**, 6683–6690 (2015).
82. Teweldebrhan, D., Goyal, V. & Balandin, A. A. Exfoliation and characterization of bismuth telluride atomic quintuples and quasi-two-dimensional crystals. *Nano Lett.* **10**, 1209–1218 (2010).
83. Xu, E. et al. Enhanced thermoelectric properties of topological crystalline insulator PbSnTe nanowires grown by vapor transport. *Nano Res.* **9**, 820–830 (2016).
84. Xu, E. Z. et al. Diameter dependent thermoelectric properties of individual SnTe nanowires. *Nanoscale* **7**, 2869–2876 (2015).
85. Hsiung, T. C., Mou, C. Y., Lee, T. K. & Chen, Y. Y. Surface-dominated transport and enhanced thermoelectric figure of merit in topological insulator $Bi_{1.5}Sb_{0.5}Te_{1.7}Se_{1.3}$. *Nanoscale* **7**, 518–523 (2015).
86. Hamdou, B. et al. Thermoelectric properties of band structure engineered topological insulator $(Bi_{1-x}Sb_x)_2Te_3$ Nanowires. *Adv. Energy Mater.* **5**, 1500280 (2015).
87. Min, Y. et al. Surfactant-free scalable synthesis of Bi_2Te_3 and Bi_2Se_3 nanoflakes and enhanced thermoelectric properties of their nanocomposites. *Adv. Mater.* **25**, 1425–1429 (2013).
88. Sun, G. L. et al. Enhanced thermoelectric performance of nanostructured topological insulator Bi_2Se_3. *Appl. Phys. Lett.* **106**, 053102 (2015).